Structure
Article

Structure and Analysis of FCHo2 F-BAR Domain: A Dimerizing and Membrane Recruitment Module that Effects Membrane Curvature

William Mike Henne,[1] Helen M. Kent,[1] Marijn G.J. Ford,[1] Balachandra G. Hegde,[2] Oliver Daumke,[1] P. Jonathan G. Butler,[1] Rohit Mittal,[1] Ralf Langen,[2,*] Philip R. Evans,[1,*] and Harvey T. McMahon[1,*]
[1] MRC Laboratory of Molecular Biology, Hills Road, Cambridge, CB1 0QH, United Kingdom
[2] Department of Biochemistry and Molecular Biology, Zilkha Neurogenetic Institute, University of Southern California, Los Angeles, CA 90033, USA
*Correspondence: langen@usc.edu (R.L.), pre@mrc-lmb.cam.ac.uk (P.R.E.), hmm@mrc-lmb.cam.ac.uk (H.T.M.)
DOI 10.1016/j.str.2007.05.002

SUMMARY

A spectrum of membrane curvatures exists within cells, and proteins have evolved different modules to detect, create, and maintain these curvatures. Here we present the crystal structure of one such module found within human FCHo2. This F-BAR (extended FCH) module consists of two F-BAR domains, forming an intrinsically curved all-helical antiparallel dimer with a K_d of 2.5 μM. The module binds liposomes via a concave face, deforming them into tubules with variable diameters of up to 130 nm. Pulse EPR studies showed the membrane-bound dimer is the same as the crystal dimer, although the N-terminal helix changed conformation on membrane binding. Mutation of a phenylalanine on this helix partially attenuated narrow tubule formation, and resulted in a gain of curvature sensitivity. This structure shows a distant relationship to curvature-sensing BAR modules, and suggests how similar coiled-coil architectures in the BAR superfamily have evolved to expand the repertoire of membrane-sculpting possibilities.

INTRODUCTION

A necessary prerequisite for motility, communication between intracellular compartments, and cell division is that cells must be able to remodel their membranes. Proteins that bind to membranes can aid this remodeling by imposing, stabilizing, or preferentially binding particular membrane curvatures. Furthermore, they can thereby dynamically recruit effector functions to specific regions of the cell. An increasing number of membrane-interacting proteins have been shown to have domains/modules that influence membrane curvature (Chitu and Stanley, 2007; Itoh and De Camilli, 2006; McMahon and Gallop, 2005). Most of these proteins that have been characterized are involved in vesicle budding and membrane trafficking. For example, during the process of clathrin-coated vesicle formation, membrane regions of distinct curvature are created and maintained. The vesicles produced are approximately 50 nm in diameter, and the necks of fully invaginated coated pits can be 20 nm or less in diameter. These curvatures are driven by a combination of membrane-interacting proteins that can directly sculpt the lipid bilayer and the clathrin scaffold that indirectly interacts with membranes and polymerizes around nascent vesicles. In this prior class, the epsin family of proteins has phosphoinositol-binding ENTH domains that, upon membrane binding, insert an amphipathic helix into the bilayer (Ford et al., 2002). This works like a wedge in the membrane and, by increasing the area of the acceptor monolayer, causes this local area of membrane to bend toward the site of insertion. Amphiphysin is another curvature-effecting protein that can function in clathrin-coated vesicle formation. This protein contains a BAR domain, where a dimeric module has a membrane-binding face with an intrinsic curvature, allowing it to stabilize membranes with this curvature (Peter et al., 2004). An additional N-terminal amphipathic helix on amphiphysin works like the amphipathic helix of ENTH domains, providing the ability to drive curvature via helix insertion. This complete module is called an N-BAR, and it has two functions, those of driving (amphipathic helix) and stabilizing (BAR) its intrinsically preferred curvature. BAR domains are not limited to roles in clathrin-coated vesicle formation, and several structures of BAR modules have now been solved (Gallop et al., 2006; Masuda et al., 2006; Peter et al., 2004; Tarricone et al., 2001; Weissenhorn, 2005). All appear rigid and prefer a similar range of curvatures.

A structural relative of the BAR module is that of the IRSp53/missing-in-metastasis homology domain (IMD) dimer. IRSp53 has a role in formation of filopodia (Millard et al., 2005). Like the BAR, the IMD is an antiparallel dimer module with each subunit folded as a three-helix bundle (Habermann, 2004; Lee et al., 2007; Millard et al., 2005). The IMD has a zeppelin-shape compared to the banana shape of BAR modules, and in vitro this protein can bind to membranes via a convex surface and can generate negatively curved membranes. It has thus been called an inverse BAR domain (I-BAR) (Mattila et al., 2007).

On sequence searches, other families of proteins show regions with low homology to BAR domains. We first recognized this BAR homology in pacsin/syndapin proteins (Peter et al., 2004). Proteins with such a homology region had previously been grouped in the *Saccharomyces pombe* cdc15 *h*omology (PCH) family of adaptor proteins (Lippincott and Li, 2000). The work of Aspenström (1997) first identified that the N terminus of all these proteins contained an FCH (*F*es and *C*IP4 *h*omology) domain followed by a coiled-coil region. These combined regions are now called F-BAR (FCH-BAR) or EFC (extended *FC*H) domains (Itoh et al., 2005; Tsujita et al., 2006). They were first described as adaptor proteins involved in the regulation of cytokinesis and actin dynamics (Lippincott and Li, 2000), but many are now implicated in membrane trafficking and are capable of membrane binding and tubulation. This has been shown in vitro in the cases of FBP17, CIP4, and Pacsin1/Syndapin1 (Itoh et al., 2005; Tsujita et al., 2006), and in vivo in the cases of Toca1, CIP4, PSPIP2, and Pacsin1/Syndapin1 (Itoh et al., 2005; Kakimoto et al., 2006; Tsujita et al., 2006). Some have C-terminal SH3 domains which bind to dynamin (see below). Several family members are also known to bind to WASP/N-WASP and have involvement in cytoskeletal dynamics, placing these proteins on an important interface in cell biology. Mutations in PCH family proteins, or in interacting partners, are also associated with autoinflammatory, neurological, and neoplastic diseases (Chitu and Stanley, 2007).

We set out to elucidate the structure of the F-BAR domain, and thus set the basis for understanding its effect on membrane curvature. We solved the structure of FCHo2 F-BAR, which is a relative of the previously studied F-BAR-containing proteins listed above, and examined the mechanism by which it can deform membranes.

RESULTS

Crescent-Shaped F-BAR Module of FCHo2

The crystal structure of residues 3–274 of hFCHo2 was determined to a resolution of 2.3 Å (Figure 1; Table 1; see Supplemental Data available with this article online). The overall structure appears crescent shaped with a shallow curvature from a side view, and tilde shaped when viewed from below (Figure 1A). Two monomers interact to form an antiparallel dimer (Figure 1A, blue/green). Each monomer is composed of five helices. The first and last helices (helices 1 and 5, respectively) of adjacent monomers lie side by side (Figure 1B). The longer helices 2, 3, and 4 form the core module, composed of a central dimerization region flanked by "wings" (Figure 1A). Helix 2 is the shortest of the core helices but runs the length of the dimerization interface and has a kink at a conserved glycine (Figure 1C). Helix 3 extends the length of the monomer, and a kink bisecting this helix occurs on the interface of the dimerization region and the beginning of the wing structure (Figure 1D). Helix 4 also runs the length of the monomer and is curved but unkinked. There is no structural discontinuity between the predicted FCH region (residues 10–94) and downstream sequences (domain marked in Figure 1F), and thus this is well described as an *e*xtended FCH (EFC) domain. The core FCH region covers helix 2 and part of helix 3, forming the central dimerization interface. The wings on each domain are more divergent, with stronger homology returning in the latter part of helix 4, where this helix rejoins the dimerization interface (Figure 1). This dimerization region is structurally conserved in BAR and I-BAR proteins, suggesting that EFC domains are another selected conformation of BAR modules, where the wings are most divergent (see below). For clarity, and to enable this conservation with BAR domains to be appreciated, we have chosen to use the term F-BAR for the complete domain. There are three molecules in the crystal asymmetric unit, comprising one dimer plus another subunit, which forms an identical dimer with its symmetry mate. The monomers superpose with root-mean-square deviations (rmsd) on Cα atoms of 0.4–0.6 Å, demonstrating that the structure is essentially rigid.

A hydrophobic dimerization interface covers a surface area of 4620 $Å^2$ (Figure 2). Most of the exposed hydrophobic residues of the monomer are buried on dimerization. The long axis of the F-BAR dimer is 195 Å, and one surface of the dimer has a very shallow concave curvature, with an arc depth of ~9 Å (Figure 1), smaller than the arc depth of ~30 Å for the classical BAR modules. In this side view, the domain can hug a circle with a curvature of greater than 110 nm in diameter. The wings of the structure are twisted away from the dimerization interface, giving the antiparallel dimer a tilde shape (~) (see bottom panel in Figure 1A). The curvature of the concave face of the dimer is generated mainly from the kinked helix 3 and the bent shape of helix 4. The less-structured N-terminal helix 1 of each monomer associates with helix 5 of its dimerization partner, forming additional interactions with helices 2 and 4 and burying conserved hydrophobic residues including Phe10 and Trp11 (Figure 1B). Helices 1 and 5 are conserved in F-BAR proteins (Figure 1F). Cys273 and Cys147 from opposing monomers form a disulfide bond in the crystal (Figure S6), which may explain the good electron density of the residues from 266 to 274.

FCHo2 F-BAR Binds to Membranes as a Dimer

To probe whether the F-BAR protein is a dimer in solution as in the crystal, we truncated our construct at residue 261 to remove the C-terminal region and the cysteine residue at position 273 that could crosslink the proteins into a dimer, if oxidized. Analytical gel filtration using the truncated protein provided evidence of dimerization (Figure 3A). The example absorbance trace from a column loaded with 130 μM F-BAR (residues 1–261) showed dimer and monomer peaks. There was no evidence of any contaminants on Coomassie-stained gels and no evidence of any aggregates larger than dimers on the column (data not shown). By analytical ultracentrifugation, the dimer dissociation constant was calculated to be approximately 2.5 μM (Figure 3B), and again we did not detect any higher-order oligomers. F-BAR domains have been shown to bind to membranes (Itoh et al., 2005; Tsujita et al., 2006), and our protein bound to Folch fraction 1 liposomes in

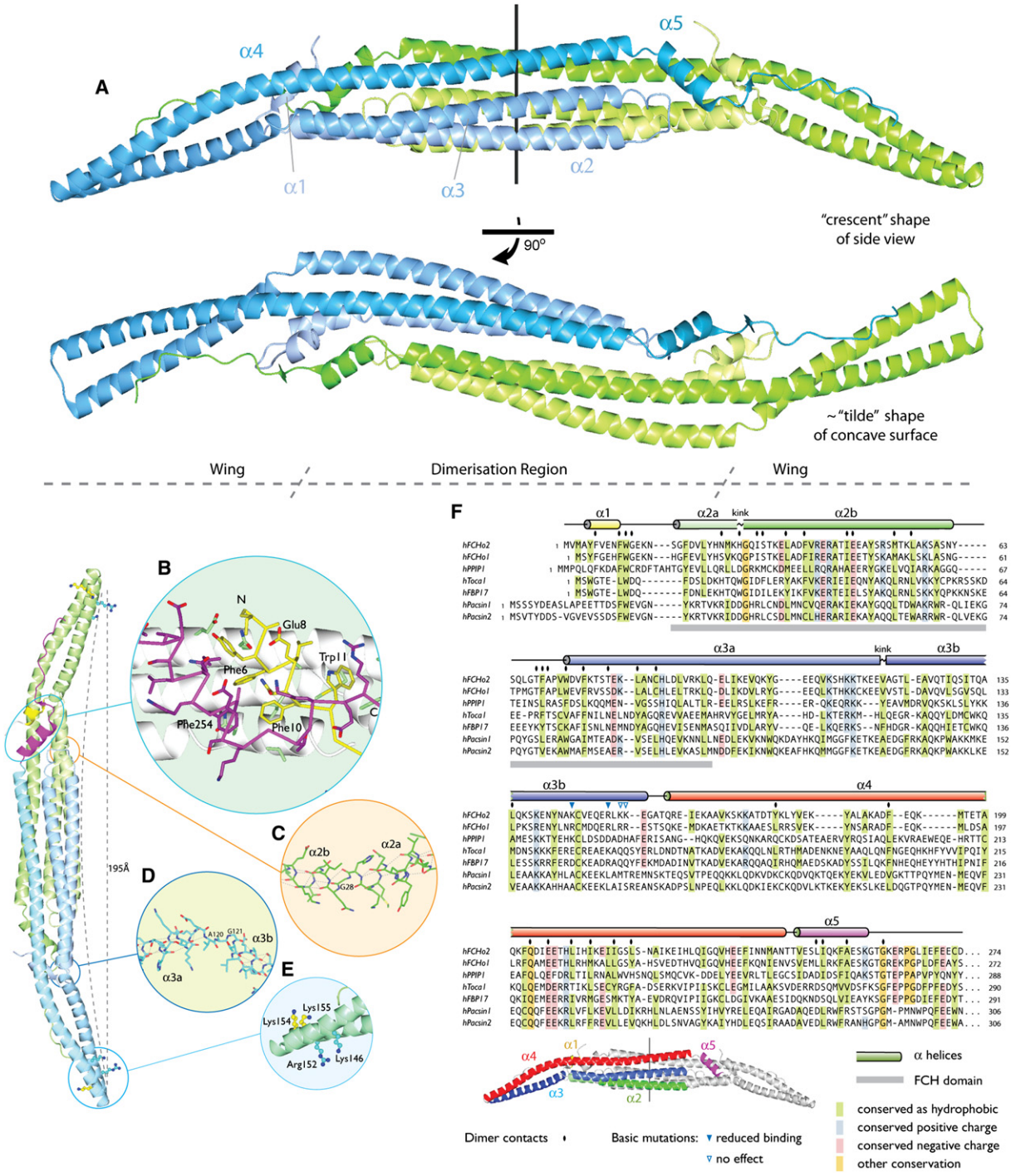

Figure 1. Structure of F-BAR Domain Dimer of Human FCH Domain Only 2

(A) Ribbon diagram of the human FCHo2 F-BAR dimeric module, residues 3–274 (Protein Data Bank [PDB] ID code 2v0o). Side and bottom views are shown. One monomer is blue and the other is green, with helices colored from N to C termini in lighter to darker hues.

(B) Packing of hydrophobic residues on helices 1 and 5 into a hydrophobic niche. α carbons and side chain of helices 1 and 5 are colored yellow and magenta, respectively. A series of hydrophobic residues lies between helices 1 and 5, including residues Phe6, Phe10, and Phe254. Glu8 resides on the exposed side of helix 1 and was used in EPR experiments.

(C and D) Details of kinks in helices 2 and 3, with hydrogen bonds displayed as dotted lines.

(E) Lysine and arginine residues mutated in this study.

(F) Structure-based sequence alignments. GenBank accession numbers for the proteins are: FCHo2, NP_620137; FCHo1, NP_620137; PPIP1, AAD11958; Toca1, AAR98814; FBP17, EAW87916; Pacsin1, NP_065855; and Pacsin2, EAW73278.

Table 1. Data Collection, Phasing, and Refinement Statistics

	Native	EMTS1	EMTS2
Data Collection			
Beamline	ID29	ID14-4	ID14-4
Wavelength (Å)	1.000	0.9795	0.9795
Resolution (Å)[a]	2.3 (2.42)	3.1 (3.27)	3.0 (3.16)
R_{merge} (highest resolution shell)[b]	0.085 (0.94)	0.118 (0.558)	0.090 (0.364)
<< I >/< σ >>	10.2 (1.6)	5.7 (1.5)	6.7 (1.7)
Completeness (%)	99.5 (99.2)	96.0 (97.9)	97.2 (98.5)
Multiplicity	3.6 (3.7)	2.1 (2.1)	2.3 (2.3)
Anomalous completeness (%)		75.5 (73.9)	75.1 (73.7)
Anomalous multiplicity		1.2 (1.2)	1.3 (1.3)
Wilson plot < B > ($Å^2$)	47		
Phasing			
Phasing power (anomalous)		1.66 (0.44)	1.55 (0.44)
R_{cullis} (centric)		0.58	0.67
Mean figure of merit (solvent flattened)	0.21 (0.79)		
Refinement			
R (R_{free})	0.251 (0.301)		
Number of reflections used (N_{free})	58,658 (3,140)		
Rmsd bond lengths (Å)	0.012		
Rmsd bond angles (°)	1.3		
Number of atoms	6,757		
< B > ($Å^2$)	66		

X-ray data collection and structure solution parameters. Crystals belonged to space group C2 with cell dimensions a = 254.4 Å, b = 65.7 Å, c = 89.9 Å, β = 110.3°.
[a] Outer resolution shell is shown in parentheses.
[b] $R_{merge} = \Sigma\Sigma\ |I_{hl} - < I_h >|/\Sigma\Sigma\ I_{hl}$.

a manner tending toward saturation in a lipid cosedimentation assay (Figure 3C). In this assay, protein that is bound to liposomes copellets with them on ultracentrifugation. The protein does not pellet in the absence of liposomes. Given that we used concentrations above the dimerization constant in solution, it is apparent that dimerization does not inhibit membrane binding as might be expected if the monomer were the membrane-interacting species. In subsequent experiments, we used concentrations of proteins and lipids that were below half-maximal protein saturation on liposomes.

To test more directly whether the dimer seen in the crystal could bind to membranes, we exploited the fortuitous disulfide bond seen in the crystal between the cysteine residues at position 147 in one monomer and 273 in the dimerization partner, and used protein from the FCHo2 3–274 construct, as used for the crystal structure, in a cosedimentation assay (Figure 3D). In the absence of a reducing agent, the protein ran as a dimer on SDS-PAGE (minus β-mercaptoethanol). In the absence of liposomes, this dimer remained entirely in the supernatant after ultracentrifugation, but with liposomes it cosedimented. A faint monomer band was seen in the presence of liposomes due to background reducing agent used during liposome preparation. When we added dithiothreitol (DTT) to an identical sample, most of the disulfide bonds were reduced and this protein bound liposomes with a similar efficiency.

Pulsed electron paramagnetic resonance (EPR) was used to test whether the dimeric structure observed in the crystal extends to the soluble and membrane-bound forms. We generated the Cys86R1 derivative of FCHo2 1–261 (see Experimental Procedures), which can be detected by EPR. In the crystal dimer, the residue Cys86 is not far from Cys86 in the dimerization partner, and thus there should be detectable spin-spin interaction between these spin-labeled sites if they are found in close proximity. The distance between the α carbons of these residues in the structure was ~20 Å, and assuming the commonly observed set of dihedral angles (χ1 and χ2 in the g+/g+ conformer) (Langen et al., 2000), a distance of around 29 Å could be expected (Figure 4A).

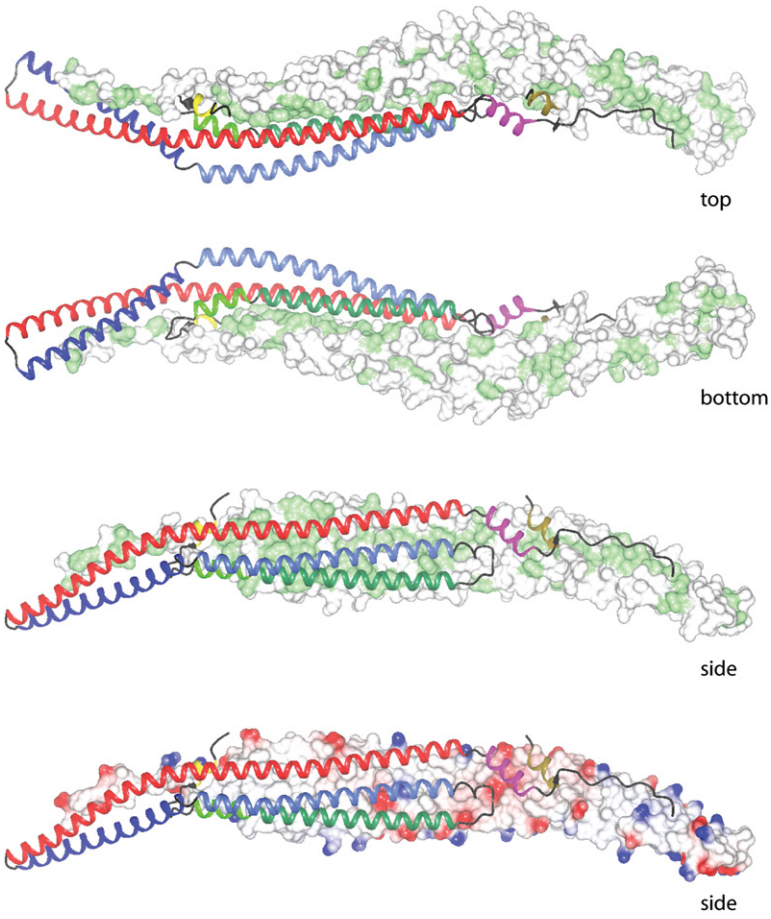

Figure 2. The F-BAR Dimer Interface Is Hydrophobic

Top, bottom, and side views with the surface of one monomer colored by residue type: hydrophobic residues (F, W, Y, P, V, A, I, L, C, M) are in green and everything else is in white. In the bottom panel the surface is colored by electrostatic potential, where red is acidic and blue is basic.

The EPR spectra for soluble and membrane-bound Cys86R1 are presented in Figure 4B. The EPR spectrum for this derivative in solution indicates a highly anisotropic motion of intermediate mobility that is consistent with its location in the X-ray crystal structure. Importantly, a very similar EPR spectrum is observed for the membrane-bound form, suggesting that membrane interaction does not cause significant conformational changes in this region. In order to obtain distance information, we employed a four-pulse double electron-electron resonance (DEER) experiment (see Experimental Procedures). In contrast to continuous-wave EPR methods that can measure distances of up to ~20 Å (Hubbell et al., 2000), this pulse EPR method extends the distance range up to 50–80 Å (Jeschke et al., 2002). Well-defined periodic oscillations are observed for the time-dependent echo intensities in solution (Figure 4C) and on membranes (Figure 4E). From the underlying frequencies of these oscillations (which are a direct measure of interspin distance), we obtained a distance of 29 Å with a rather narrow distance distribution for both the soluble and membrane-bound forms of the Cys86R1 derivative (Figures 4D and 4F). This distance is in agreement with the crystal structure, suggesting that the crystal-like dimer is likely retained in solution and on membranes.

Concave Membrane-Binding Face of the F-BAR Module

There are at least 25 positively charged residues on the shallow concave face of the F-BAR dimer (Figure 5A). Such clustering of positively charged residues occurs on the lipid-binding concave face of amphiphysin BAR and other BAR modules (Peter et al., 2004). However, there is also a patch of negatively charged residues in a central groove of the concave face of the F-BAR. To test whether membrane binding involved basic residues on the concave surface, as we found in the BAR module, we made a double lysine/arginine mutant Lys146Glu+Arg152Glu (Figure 1F), thus reversing the charge of four residues on this surface of the dimer. This reduced membrane binding by approximately 40% (Figure 5B). In contrast, a Lys154-Glu+Lys155Glu mutant (where the mutated residues are on the convex face of the F-BAR dimer) failed to reduce membrane binding (Figure 5B). These results are similar to those from experiments in amphiphysin and endophilin, where double mutants of positively charged residues on their concave faces reduced membrane binding but did not completely abolish the interactions.

In endophilin, the BAR domain begins at residue 30, but residues N-terminal to this fold into an amphipathic helix upon membrane binding by the N-BAR module. The

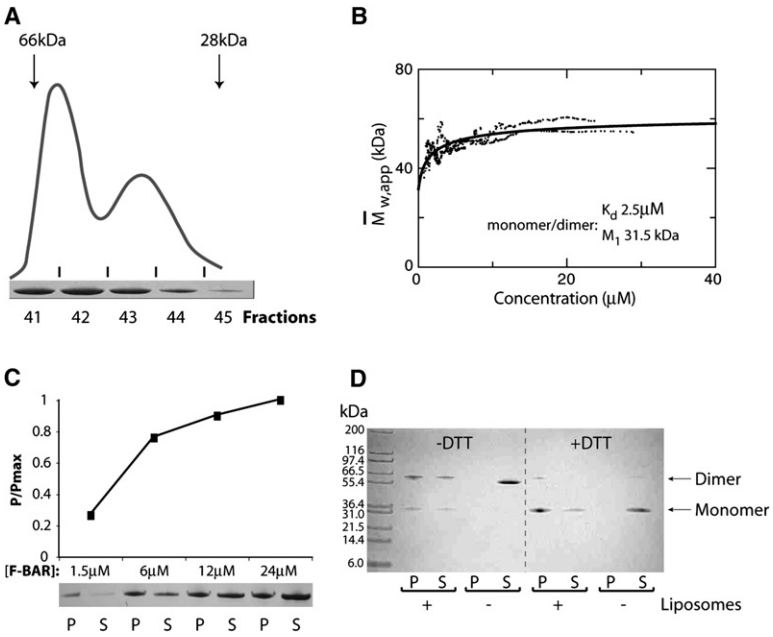

Figure 3. The F-BAR Dimer Binds to Membranes

(A) The F-BAR domain of FCHo2 eluted as a twin peak on analytical gel filtration using a Superdex 200 column; 130 μM mFCHo2 (residues 1–261) was loaded. Fraction 40 was calibrated to 66 kDa BSA and fraction 45 was 28 kDa GST. The larger peak runs at about 60 kDa, and the smaller peak > 30 kDa, are consistent with a monomer:dimer equilibrium of a protein having a predicted monomer mass of 30 kDa.

(B) Analytical ultracentrifugation of FCHo2 F-BAR domain showed a monomer:dimer equilibrium in solution with a K_d of 2–8 μM.

(C) The F-BAR domain of mFCHo2 bound liposomes in a saturable manner. Liposomes were made from Folch fraction 1 and extruded through a 0.8 μm filter. Cosedimentation with 0.5 mg/ml liposomes was quantified from the Coomassie-stained gel. P, pellet; S, supernatant. At protein concentrations above 24 μM, there was significant nonspecific protein aggregation.

(D) The crystal dimer of FCHo2 binds membranes. The crystallized F-BAR domain was concentrated in the absence of the reducing agent DTT to generate a constitutive dimer like that in the crystal from two disulfide bonds between Cys147-Cys273 in the adjacent monomers (see Figure S6). This sample pelleted with 0.5 mg/ml 0.8 μm filtered Folch liposomes, and ran as a dimer of ~62 kDa on SDS-PAGE gel. The protein did not pellet in the absence of liposomes. The addition of DTT released the constitutive dimer, which still pelleted with 0.8 μm filtered liposomes, and ran as a monomer on SDS-PAGE gel. It appears that higher concentrations of the dimer migrate slightly further on SDS-PAGE.

hydrophobic face of this helix becomes structured and inserts into the lipid bilayer, and flanking positively charged residues are positioned at the level of the negatively charged 1-phosphates of phospholipids (Gallop et al., 2006). Given the potential amphipathic nature of the initial residues of the F-BAR domain, we asked whether they may also contribute to the membrane interaction. However, in our F-BAR crystal structure (residues 3–274), residues 4–11 already form an α helix (helix 1) that interacts with helix 5 of the adjacent monomer. As would be expected, we found no evidence of any change in α helicity by circular dichroism spectroscopy upon membrane binding (data not shown), and thus this region is likely a constitutive helix. To test for a role for helix 1 in membrane binding, we deleted this helix and assayed whether the protein could be more easily displaced from membranes with buffers of increasing ionic strength (Figure 5C). We used two amphiphysin constructs as controls, the N-BAR module (residues 1–244) and the BAR module (residues 27–244, missing the N-terminal amphipathic helix). The complete N-BAR module was not displaced by increasing salt concentration, likely due to hydrophobic insertions of residues on the amphipathic helix, but the BAR module was easily displaced, confirming the ionic nature of the BAR interaction. The F-BAR module was intermediate in its displacement characteristics, and helix 1 deletion resulted in a mild increase in salt sensitivity, suggesting that whereas the F-BAR interaction is predominantly ionic, there may be a small contribution from hydrophobic residues.

Helix 1 Is Structured in Solution and on Membranes

To obtain further structure information on the N-terminal residues of F-BAR, we introduced spin labels at residues Val2 and Glu8. Our structure starts at residue 3, but we predicted that valine 2 should be accessible for labeling, and glutamate 8 is also exposed on helix 1 and so can also be labeled. The EPR spectra of both spin-labeled derivatives in solution exhibited intermediate mobility (Figure 5D, black traces). Thus, in contrast to the high mobility observed in the case of endophilin N-terminal residues (Gallop et al., 2006), these data indicate that residues 2 and 8 are part of an ordered structure. Similarly, both sites were also part of an ordered structure upon membrane interaction (Figure 5D, red traces). To assess whether the N terminus participates in membrane interaction, we recorded the accessibility of the labeled Val2R1 and Glu8R1 derivatives to O_2 and NiEDDA. Extensive previous data have shown that R1 accessibility to O_2 increases with increasing immersion depth in the membrane, whereas R1 accessibility to NiEDDA decreases under those conditions. This allows the ratio of the O_2 and NiEDDA accessibilities of a given membrane-exposed site (typically expressed by the contrast parameter Φ) to be used as an indicator of membrane immersion depth. We found that Val2R1, but not Glu8R1, exhibits elevated O_2 accessibility and reduced NiEDDA accessibility upon membrane interaction. Based upon the Φ value of 1.1 for the Val2R1 derivative, the nitroxide moiety is membrane inserted at a depth of approximately 3 Å. These data show that the N terminus is capable of interacting with the

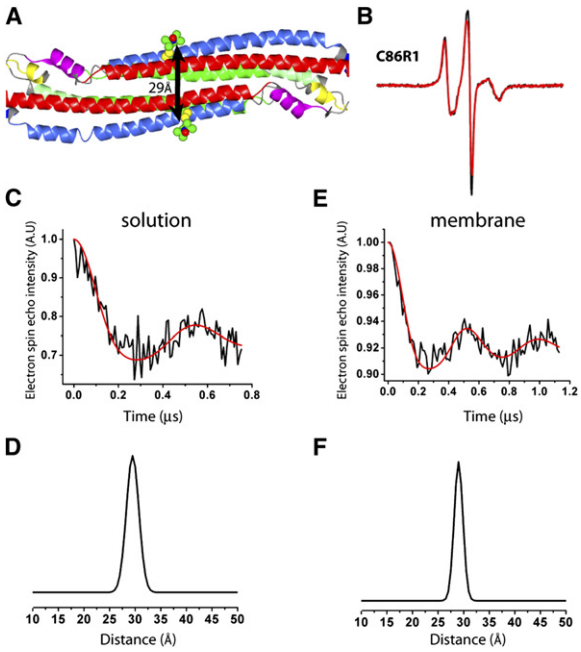

Figure 4. Electron Paramagnetic Resonance Shows a Dimer on Membranes

(A) Site-directed spin labeling of residue Cys86 of mFCHo2 F-BAR protein (residues 1–261) in which Cys147 was mutated to Ser. The location of Cys86 within the respective dimer subunits is shown. The crystallographic distance between the α carbon atoms is ~20 Å. The labeled Cys86 side chains are shown in space-fill representation using the g+/g+ (χ1/χ2) rotameric states, which were commonly observed at helix surface sites in crystals of spin-labeled T4 lysozyme derivatives (Langen et al., 2000). The resulting nitroxide-nitroxide distances are on the order of ~29 Å.

(B) EPR spectra for Cys86R1 F-BAR in soluble (black) and membrane-bound forms (red). Scan width is 150 Gauss.

(C–F) The baseline corrected time evolution data from a four-pulse DEER experiment of Cys86 in solution (C and D) and when bound to membranes (E and F). The red lines represent the best fit to the data in (C) and (E), and (D) and (F) give the resulting distance distributions.

membrane, but at least for the sites tested it is not inserted as deeply as the amphipathic helices of N-BARs. For comparison, the hydrophobic residues of endophilin amphipathic helix have Φ values of up to 2.0 (Gallop et al., 2006). The lack of deep insertion for Val2 correlates with the absence of positively charged residues flanking the hydrophobic surface of the helix.

Membrane Tubulation and Curvature Sensitivity

BAR modules show a binding preference for highly curved membrane interfaces (Peter et al., 2004), which is a result of the curvature of the concave face (Gallop et al., 2006; Masuda et al., 2006). In contrast, N-BAR modules bind different-sized liposomes without preference, as they impose their own curvature on membranes via N-terminal helix insertion (Gallop et al., 2006; Masuda et al., 2006; Peter et al., 2004). As the F-BAR module also has a concave curvature, but of a distinctly different arc depth to the BARs, we examined the binding of wild-type and mutant F-BAR modules to liposomes of different sizes. Like the N-BAR, the F-BAR wild-type module bound equally to all liposome sizes tested (Figure 5E). The Lys146Glu+Arg152Glu mutant on the concave face reduced liposome binding (Figure 5B) but also showed no curvature preference (Figure 5E). A double Lys mutant on the convex surface did not affect binding. Deletion of helix 1 caused the F-BAR module to bind to liposomes in a curvature-sensitive manner (data not shown). However, this is a severe mutation, causing exposure of hydrophobic residues. We therefore made a point mutation on this helix: Phe10Glu. This protein also showed curvature-sensitive liposome interactions (Figure 5E). Interestingly, it bound less well to smaller liposomes; this is the opposite curvature preference than was seen for the BAR domains of both amphiphysin and endophilin. A curvature preference of Phe10Glu for larger liposomes implies that the F-BAR module does not stabilize extreme positive curvatures, but by analogy with the N-BAR domain, the curvature insensitivity of the wild-type F-BAR suggests that it can impose its curvature on membranes. Tubulation by F-BAR domains has previously been reported for other family members (Itoh et al., 2005; Tsujita et al., 2006), and thus we tested FCHo2 F-BAR for its ability to tubulate liposomes by examining protein-bound liposomes by electron microscopy (EM).

The F-BAR domain tubulated Folch liposomes, extruded through a 0.8 μm filter, to a mixture of broad-diameter, cigar-like tubules (~130 nm) and more heterogeneous but narrower tubules of 20 nm and above (Figure 6A). There were relatively few broad tubules, but they were uniform in diameter, and occasionally long versions of the tubules were observed (Figure 6B). A visible coat could be identified (Figure 6C), and some large tubules appeared to be in the process of being formed where elongated liposomes showed upturned rims (see example in Figure 6D). These samples are negatively stained and dehydrated before microscopy, and this could explain the flat appearance of some large tubules (Figure 6C). With small liposomes, extruded through a 50 nm filter, we found no broad tubules, but narrower tubules were still produced (Figure 6E). Individual small liposomes often had multiple sprouts of narrow tubules (Figure 6E). It is clear from these micrographs that the narrower tubules were of very variable diameters along their lengths, and thus are unlikely to arise from precise packing of the F-BAR protein.

We next tested the Phe10Glu mutant of helix 1, which we have shown to be curvature sensitive, binding preferentially to larger liposomes (Figure 5E). Notably, with Phe10Glu there was still tubulation, but we found very few examples of narrow tubules (Figures 6F and 6G). Given that curvature driving and curvature sensing are opposite ends of a continuum, it is not surprising that there are fewer narrow tubules. Changes in curvature sensitivity may therefore be a more quantitative assay for changes in tubulation efficacy. To our knowledge, this is the first report of narrow tubules being generated by an F-BAR module. It may well be that these narrow tubules are much

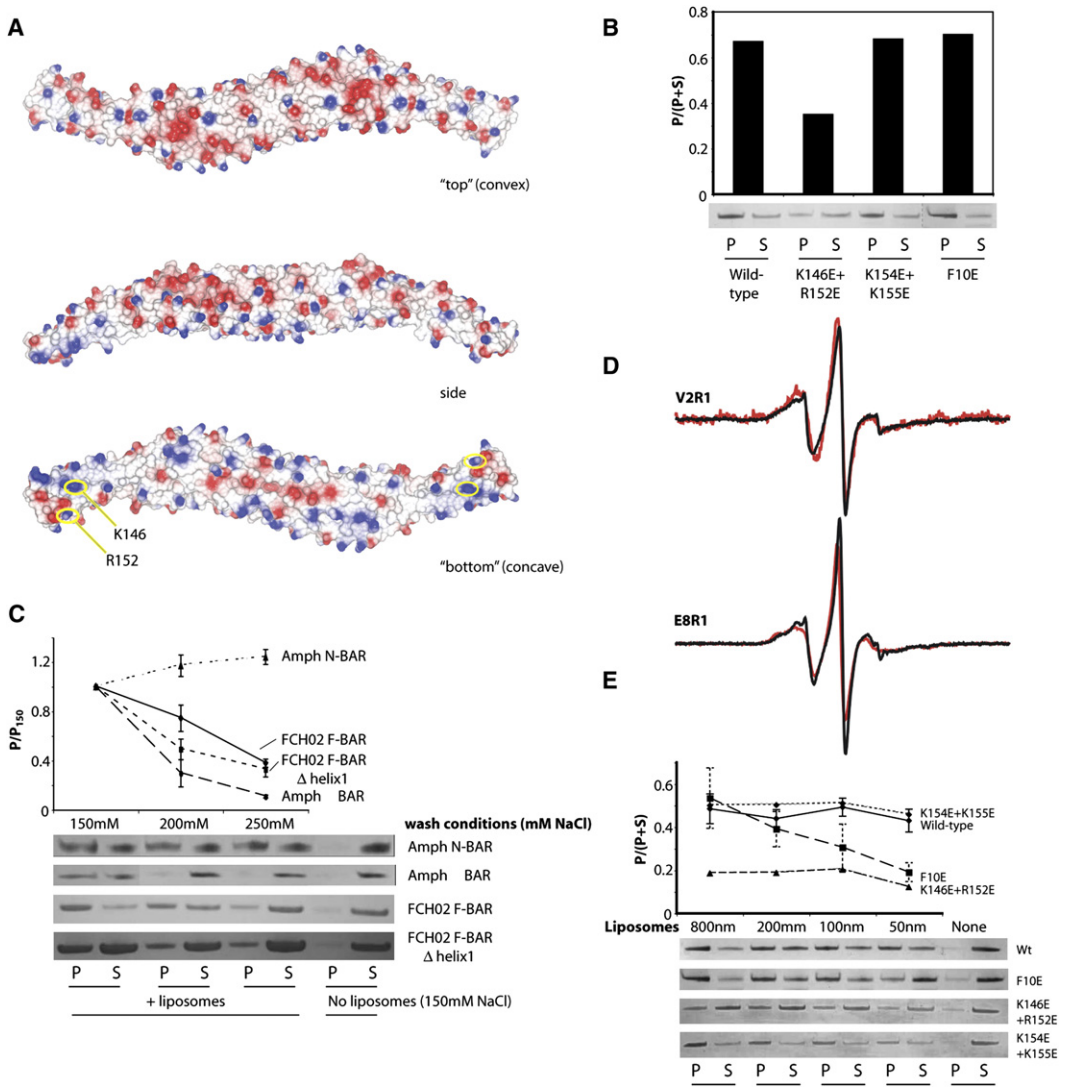

Figure 5. The FCHo2 F-BAR Domain Binds Membranes via Its Dimeric Concave Face

(A) Surface representation of the FCHo2 F-BAR module colored according to electrostatic potential. Colors are red, negatively charged Glu/Asp residues to blue, positively charged Lys/Arg/His residues, in the range of −0.5 to 0.5 V. The concave face (bottom panel) is polydispersed with a higher concentration of positively charged residues, whereas the convex face (top panel) has a lower positive charge distribution.

(B) The F-BAR dimer module binds liposomes via its concave face. Cosedimentation assays of 0.8 μm Folch liposomes and F-BAR Lys/Arg mutant Lys146Glu+Arg152Glu (dimer concave face mutations) demonstrate 42% reduction in pelleting as compared to wild-type F-BAR protein. Mutant Lys154Glu+Lys155Glu (dimer convex face) shows no reduced pelleting. A Phe10Glu mutation in helix 1 does not affect pelleting. Protein concentrations are 4 μM. P, pellet; S, supernatant. There was no pelleting of protein in the absence of liposomes.

(C) FCHo2 F-BAR domain interaction with lipid membranes is largely ionic. Salt wash assays were conducted with wild-type and helix 1 deletion of the F-BAR module protein. A 5 min 200 mM NaCl salt wash causes a 26% (±10%) reduction in wild-type protein pelleting. A 250 mM salt wash results in a 62% (±3%) reduction in wild-type pelleting. Deletion of helix 1 (Δhelix 1) of F-BAR exacerbates this decline. *Drosophila* amphiphysin (d-Amph) N-BAR domain (residues 1–244) and BAR domain alone (residues 27–244) were used as controls. The results are the mean ± SEM of three independent experiments.

(D) X-band EPR spectra of F-BAR derivatives labeled with spin label R1 at the indicated positions. Spectra obtained from protein in aqueous solution are shown in black and those of membrane-bound F-BAR are shown in red. The scan width is 150 Gauss. All spectra are consistent with the location of the spin labels in an ordered structure.

(E) Mutation of helix 1 hydrophobic residue Phe10Glu causes the FCHo2 F-BAR module to bind better to larger liposomes. F-BAR protein was co-pelleted with 0.5 mg/ml Folch fraction 1 liposomes that had been extruded through filters with pore diameters of 0.8, 0.2, 0.1, and 0.05 μm. Wild-type F-BAR domain pellets equally with all liposome sizes. The Phe10Glu mutant protein showed curvature sensitivity as compared to wild-type protein, with 56% (±4%) less pelleting with 0.05 μm filtered liposomes. Lys146Glu+Arg152Glu mutant protein showed less total pelleting for all liposome sizes (average 35% reduction versus wild-type), and no preference for liposome size. Lys154Glu+Lys155Glu mutant protein also showed no preference for liposome size, and pelleted equally well compared to wild-type protein. Protein concentration for experiments was 2–4 μM. The results are the mean ± SEM of three independent experiments.

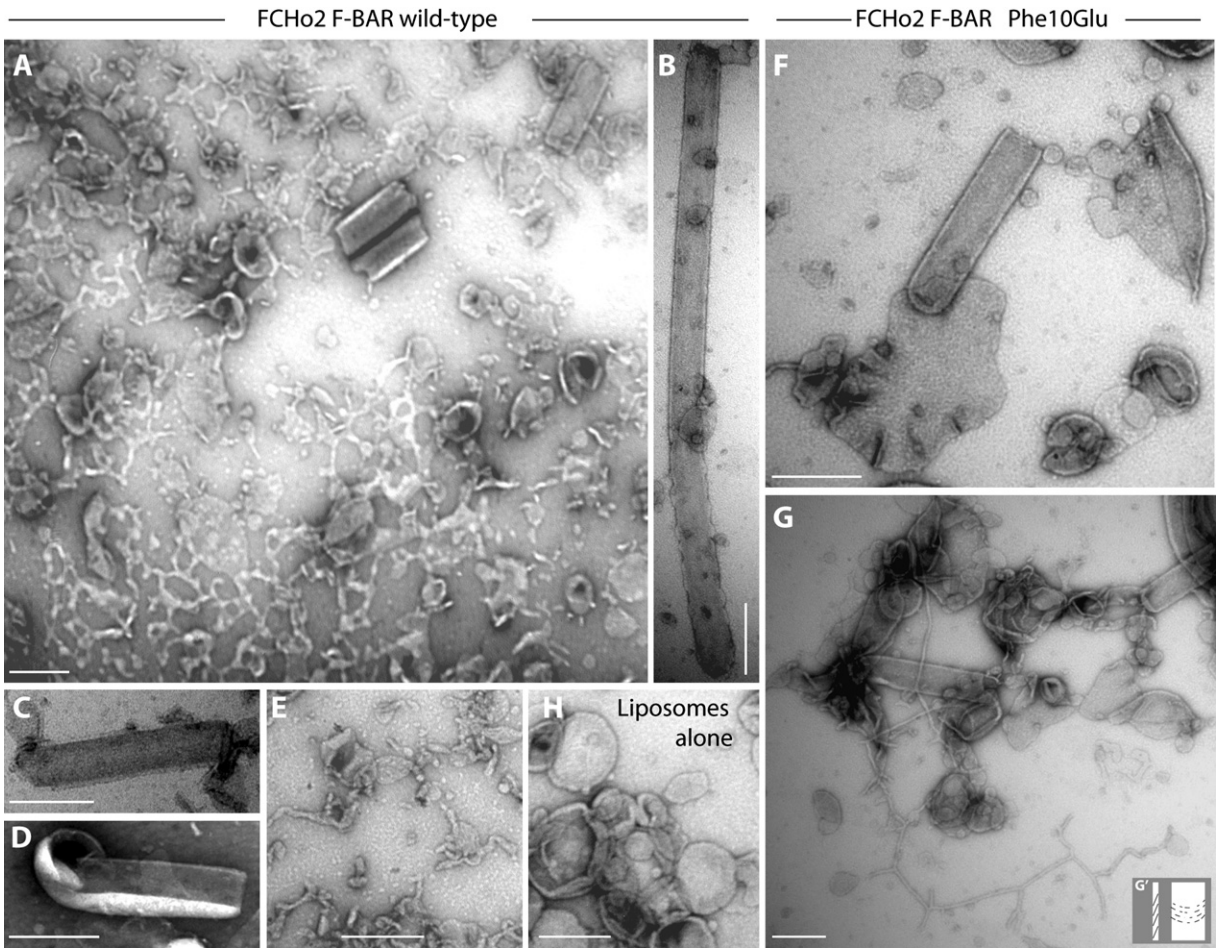

Figure 6. The F-BAR Domain of FCHo2 Deforms Folch Liposomes into Tubules with a Range of Diameters

Micrographs of Folch fraction 1 liposomes coincubated with F-BAR modules.

(A) Wild-type F-BAR module tubulated 0.8 μm filtered liposomes. Tubules varied from large tubules with a flat appearance and diameter of approximately 130 nm to smaller tubules with a lower diameter of approximately 25 nm.

(B) Example of a long tubule with a flat appearance.

(C) Visible coat at the edges of a tubule.

(D) Tubulogenesis: F-BAR module deforms a liposome into a tubule.

(E) Wild-type F-BAR domain tubulation of 0.05 μm filtered liposomes into only narrow tubules of approximately 25 nm diameter. These tubules are sometimes interconnected, and multiple tubules can come from the same small liposome.

(F and G) Helix 1 point mutant Phe10Glu shows both types of tubules, but smaller tubules are harder to find. Insert shows possible orientation of the F-BAR module to achieve these different tubule diameters (G′).

(H) Control Folch fraction 1 liposomes without addition of protein.

The scale bars represent 200 nm.

more unstable. We have seen examples where they have fused to each other, but they may also fragment due to their extreme curvature (Figure 6A).

Given the twisted shape of the F-BAR module, the diameter of a tubule on which this protein would comfortably sit in an approximately tangential manner is around 110–130 nm, which is close to the diameter of the large tubules seen by EM. If the F-BAR were at a more oblique angle to the axis of the tubule, then the diameter accommodated would be narrower (Figure 6G′). Thus, the FCHo2 F-BAR module can accommodate variable diameters up to approximately 130 nm.

The Structurally Defined F-BAR Domain Protein Family

Our structure has now allowed us to accurately extend the F-BAR family, and thus we have listed the human F-BAR-containing proteins identified from our analysis (Figure 7). F-BAR domains are preferentially found at N termini of proteins but not exclusively, as GAS7 and hMHA1 have F-BAR domains at the C terminus and middle, respectively. There should be no structural reason why the F-BAR cannot be located at the middle or the C terminus of a protein, given that both the N and C termini of the module are likely to be free to continue without disrupting

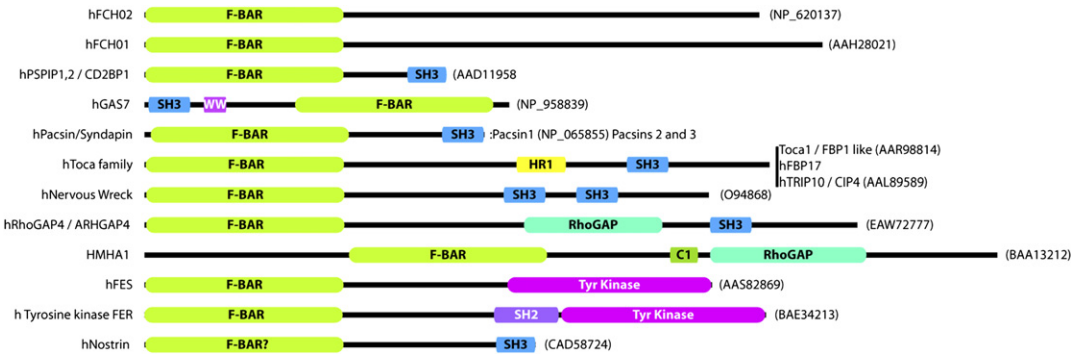

Figure 7. The F-BAR Domain Is the Unifying Feature of the PCH Family

Domain schematic of human PCH family proteins, listed by their degree of homology to human FCHo2. PSPIP, proline-serine-threonine phosphatase interacting protein 1 (hPSPIP2 has no SH3 domain); GAS7, growth arrest suppressor 7; Toca1, transducer of Cdc42-dependent actin assembly 1; FBP17, forming-binding protein 17; TRIP10, thyroid hormone receptor interactor 10 variant, also called Cdc42-interacting protein 4 (CIP4), and also called Felic; SLIT-ROBO Rho GTPase activating protein has the same domain structure as RhoGAP4; HMHA1, minor histocompatibility antigen 1 and hGEM interacting protein have the same domain structures.

membrane association. However, if the ability of helix 1 to change conformation is important for membrane binding, then this helix may well prefer to be at the N terminus.

BAR domains are frequently coupled to other direct membrane recruitment modules (such as PH or PX domains). These work synergistically to localize the proteins to membranes of specific composition and curvature (Carlton et al., 2004; Peter et al., 2004), but it is interesting to note that this synergy is not a prominent feature of F-BAR proteins. Overall, F-BAR family proteins play diverse and significant roles as both effectors and regulators in cytoskeletal and endocytic processes in the cell through indirect and direct association with the cytoskeleton and endocytic proteins (Table 2).

The BAR Superfamily

The F-BAR, BAR/N-BAR, and I-BAR domains are structurally similar homodimeric modules with antiparallel arrangement of monomers (Figure 8). They all share a common central core region of extended α helices, where the cores of all three domains can be overlaid with a high degree of architectural conservation (Figure 8, bottom panel). However, the flanking wing regions differ. The angle of dimerization and conserved kinks produce these wings of varying splay. The dimerization interface of the F-BAR covers a solvent-accessible area of 4620 Å^2. When the additional helices 1 and 5 (which are less well ordered than the central dimerization core) are not included in the calculation, then the area buried is 2150 Å^2. This is comparable to the BAR module of amphiphysin (2410 Å^2) and the BAR module of endophilin (2800 Å^2), and the K_ds of all are in a similar range. The I-BAR module contains wings in the same plane as the α helices of its core region, producing a flat zeppelin- or lens-like structure. In the F-BAR module, a kink in helix 3 and a bend in helix 4 generate a shallow concave face that is of intermediate splay compared with BAR and I-BAR modules. The same helices have kinks in the BAR module, and extra curvature is achieved by having a less antiparallel dimerization interface (Figure 8).

BAR modules from at least three different protein families have been solved, and they can all be overlaid with a high degree of architectural conservation. The central dimerization cores are almost identical, but the wings are slightly contorted with respect to each other. The same will likely be true for F-BAR modules. An overlay of cross-sections through the axis of symmetry of each of the three domains shows that the different helices are in approximately the same position (Figure 8). Taken together, our data suggest that the F-BAR module is indeed a member of a larger BAR superfamily.

DISCUSSION

Unlike the previously studied F-BAR-containing proteins, FCHo1 and 2 (FCH domain only 1 and 2), as the names suggest, contain no C-terminal SH3 domain nor any other known domains. The central and C-terminal regions are predicted to be largely disordered, but the last 300 amino acids are conserved across species and homologous to a region in endophilin interacting protein-1. Homologs of FCHo2 exist among mammalian, *Drosophila*, and *Caenorhabditis elegans* genomes, and human *FCHo2* has been characterized in situ as a 26-exon gene on chromosome position 5q13.2 (Katoh and Katoh, 2004).

The F-BAR module of FCHo2 is a dimeric membrane-binding curvature effector. Its interaction with membranes was found to be largely ionic and via a shallow concave face. It deformed liposomes into a range of tubule diameters from 20 to 130 nm, where variable diameters may be achieved by orientating the F-BAR module at various oblique angles relative to the tubule axis. As in the case of amphiphysin (Peter et al., 2004), the curvature preference is obscured in the wild-type protein, because tight binding allows the protein to deform liposomes to match their preference. Mutation of the N-terminal helix (Phe10Glu

Table 2. F-BAR Family Members and Proposed Functions

Protein	WASP/N-WASP Interaction	Function
FCHo1/2		Unknown
PSPIP1/2	Yes	Cytoskeletal reorganization and role in macrophage motility (Ferguson et al., 2006; Grosse et al., 2006)
GAS7		Cytoskeletal reorganization, seen in neurite outgrowth of Purkinje neurons (Chao et al., 2005)
Pacsin/syndapin	Yes	Cytoskeletal reorganization effector via N-WASP; also endocytic role via dynamin1 and synaptojanin interactions (Qualmann et al., 1999)
Toca1 family	Yes	Actin cytoskeletal reorganization (Ho et al., 2004); plasma membrane recruitment of endocytic proteins for FBP17 (Tsujita et al., 2006)
Nervous wreck	Yes	Regulates *Drosophila* neuromuscular junction growth via Wsp (Coyle et al., 2004)
RhoGAP4		Stimulates GTP hydrolysis of Rac1, Cdc42, and RhoA (Foletta et al., 2002)
HMHA1		Potential RhoGTPase effector
FES		Monomeric tubulin binder and microtubule reorganization effector; potential proto-oncogene (Delfino et al., 2006)
FER		Role in cell-cell associations at adherens junctions (Kim and Wong, 1995) potential proto-oncogene (Pasder et al., 2006)
Nostrin	Yes	Trafficking of nitric-oxide synthase (eNOS); may be caveolin associated (Schilling et al., 2006)

mutation in FCHo2, or deletion of the N-terminal helix in amphiphysin) weakens the binding and uncovers the intrinsic preference, for small liposomes (<100 nm) in the case of amphiphysin and for large liposomes for FCHo2. These different preferences correspond to the approximate curvatures accommodated by the concave face of the modules.

The dimeric nature of the F-BAR architecture means that other domains within F-BAR-containing proteins are presented as pairs on a membrane surface, and this may well increase their avidity for ligands, making these effective recruitment proteins. Curvatures induced by various BAR modules represent the most extreme positively curved membranes observed in vivo. Having another module, the F-BAR, that can induce or accommodate a less extreme positive curvature broadens the repertoire of membrane-sculpting possibilities. It may also point to the existence of other modules with yet different curvature preferences.

EXPERIMENTAL PROCEDURES

Protein Expression and Purification

Human (hFCHo2, residues 3–274) and mouse (mFCHo2, residues 1–261) constructs were cloned into pGEX-6P1 and transformed into *Escherichia coli* Rosetta or BL21 *pLysS* strains. Protein was harvested following overnight induction with 50 μM IPTG at 25°C. GST-tagged protein was purified from the bacterial lysate using GSH Sepharose beads (GE Healthcare). The beads were washed with HN buffer (150 mM NaCl, 20 mM HEPES [pH 7.5], 2.5 mM DTT), and the GST tag was cleaved off overnight with PreScission protease (GE Healthcare). Protein was further purified on a Superdex 200 gel-filtration column (GE Healthcare) and concentrated.

Protein Crystal Optimization, Data Collection, Phasing, Refinement, and Model Building

hFCHo2 protein was concentrated to a minimum of 5 mg/ml. Crystals were obtained using sitting drop vapor diffusion against a reservoir containing 18% PEG 4000, 300 mM sodium acetate, and 100 mM Tris (pH 9) at room temperature. Crystals appeared after 24 hr and grew to typical dimensions of approximately 0.4 × 0.2 × 0.2 mm. For cryocooling, crystals were transferred stepwise into the crystallization condition supplemented with up to 24% glycerol. Derivative crystals were generated by soaking the crystals in mother liquor supplemented with 1 mM ethyl mercury thiosalicylate (EMTS) for variable lengths of time ranging from 30 min to several days.

Native and derivative data were collected at ID14-4 and ID29 at the European Synchrotron Radiation Facility in Grenoble, France. Crystals belonged to space group C2 with cell dimensions a = 254.4 Å, b = 65.7 Å, c = 89.9 Å, β = 110.3° and had three molecules in the asymmetric unit, forming one and a half dimers (i.e., with one dimer related by the crystallographic dyad). The intensities were markedly anisotropic: native data extended to 2.3 Å along a* but not much beyond 2.8 Å in the other directions (eigenvalues of the anisotropic distribution of |F| = 0.35, 0.65, 1.0). The two derivative data sets were each somewhat incomplete (see Table 1), but together they covered nearly all reflections to 3.1 Å resolution. Reflections were integrated with MOSFLM (Leslie, 2006) and scaled with SCALA (Evans, 2006) from the CCP4 suite of crystallographic software (CCP4, 1994). The two mercury crystals were treated as separate derivatives. Heavy-atom sites were found using SHELXD (Uson and Sheldrick, 1999), called from the autoSHARP procedure (Bricogne et al., 2003). The substructure was completed and refined using SHARP (de la Fortelle and Bricogne, 1997). Following solvent flattening using SOLOMON (Abrahams, 1997) with 60% solvent, the experimental map was clearly traceable. The model was built using O (Jones et al., 1991) and Coot (Emsley and Cowtan, 2004) and was refined using REFMAC5 (Murshudov et al., 1997).

Liposome Preparation and Cosedimentation Spin Assays

Folch fraction 1 liposomes (Sigma) were mixed in a 3:1 ratio of methanol:chloroform and evaporated in a glass tube with a gas stream of argon. After vacuum desiccation to ensure the complete removal of solvent, liposomes were hydrated in HN buffer to a concentration of 1 mg/ml. They were then sequentially passed through Nuclepore polycarbonate filters (Whatman) by syringe extrusion through the following filters: 0.8, 0.2, 0.1, and 0.05 μm. In cosedimentation assays, protein was added to 0.5 mg/ml (final concentration) liposomes in HN buffer for 30 min at room temperature in Beckman 7 × 20 mm polycarbonate tubes and spun down in an Optima TL desktop ultracentrifuge. Pellet and supernatant fractions were resuspended in equal volumes of sample buffer, and run on 4%–12% Tris SDS-PAGE gels (Invitrogen). For

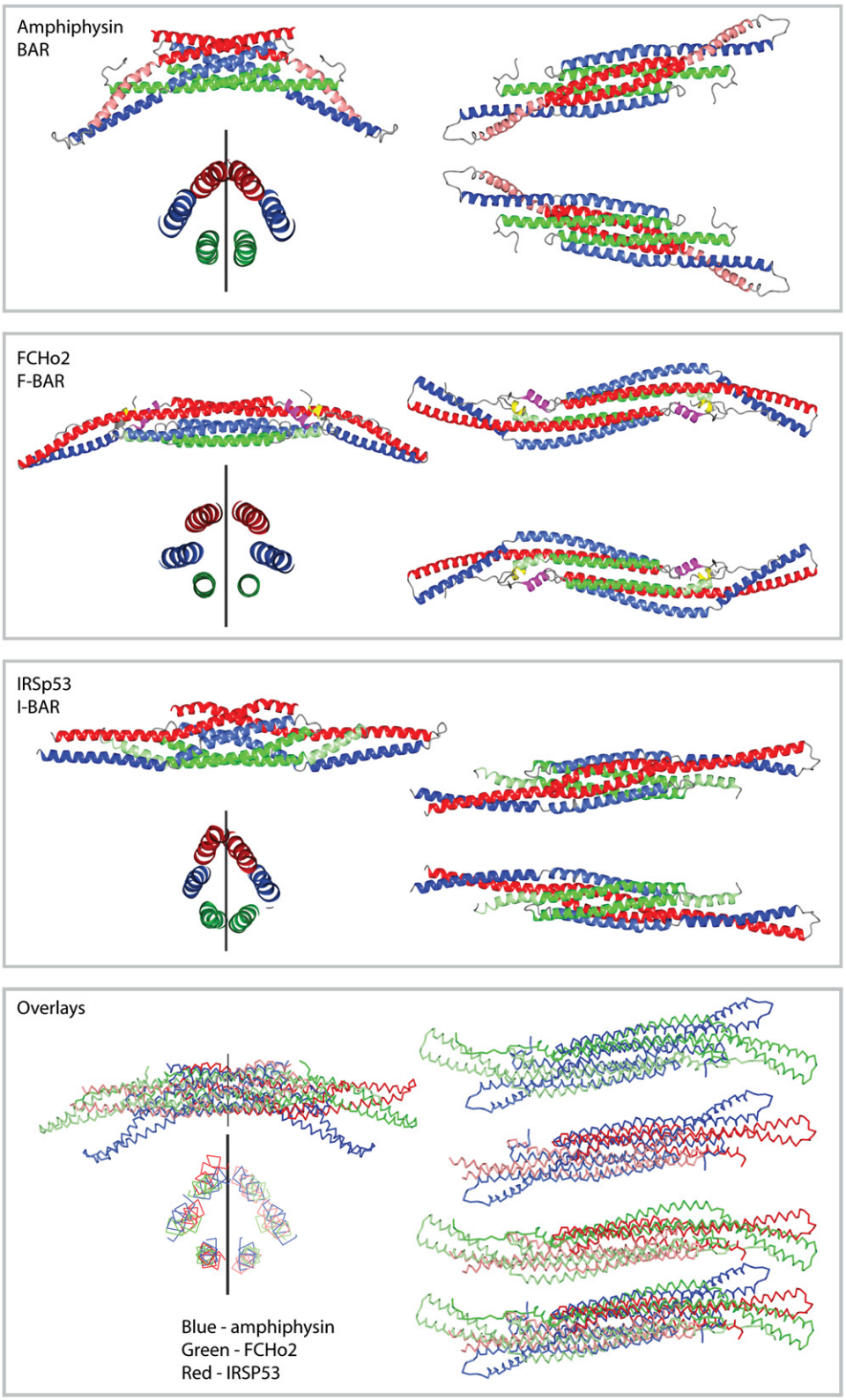

Figure 8. The BAR Superfamily

Structural similarities between the BAR family, FCHo2 F-BAR family, and I-BAR family. Amphiphysin BAR structure (PDB ID code 1uru), the founding member of the superfamily, is compared with FCHo2 F-BAR (PDB ID code 2v0o) and IRSp53 I-BAR (PDB ID code 1y2o) structures. Overlays show the central dimerization core aligns well, but the wings are splayed at different angles, providing divergent membrane curvature binding preferences.

experiments involving the use of the disulfide-linked dimer, DTT was omitted. Experiments testing for curvature sensitivity used Dab2 PTB domain (curvature-insensitive lipid-binding domain) to control for the amount of available liposome (data not shown). For experiments involving salt washes, protein-liposomes were allowed to incubate for 30 min, and then NaCl was added to a final concentration of 200 or 250 mM for 5 min and immediately spun down.

Equilibrium Ultracentrifugation

Please see Supplemental Data.

Spin Labeling and EPR Spectroscopy

N-terminal single-cysteine mutants, Val2Cys and Glu8Cys, were generated in an otherwise cysteine-free background, in which the native cysteines (Cys147 and Cys86) were replaced with serines. The Cys86 single-cysteine mutant was made by replacing Cys147 with serine. Purified single-cysteine mutants in HN buffer were subjected to size-exclusion chromatography (PD-10 column; Amersham Biosciences) in buffer to remove DTT. Immediately following DTT removal, proteins were labeled with a 10-fold molar excess of an MTSL nitroxide spin label ([1-oxyl-2,2,5,5-tetramethylpyrroline-3-methyl]-methanethiosulfonate) to generate the new side chain R1. After 1 hr incubation, unreacted label was removed by size-exclusion chromatography (PD-10 column; Amersham Biosciences).

EPR spectra at room temperature were recorded using X-band Bruker EMX spectrometers that were fitted with a Bruker ER4119HS resonator (12.7 mW power). The scan width for the magnetic field was 150 Gauss. Membrane-bound samples were generated by incubating 30 μg of protein with 700 μg of extruded 400 nm Folch liposomes in a total volume of 1.5 ml. For all samples, membrane interaction was verified by a copelleting assay. Whereas no pelleting was observed at 210,000 × g in the absence of membranes, nearly quantitative pelleting occurred in the presence of liposomes. The same copelleting method was also used as a means of concentrating membrane-bound F-BAR for EPR analysis (final volume 10–20 μl). Accessibility to oxygen (from air; Π [O_2]) or 10 mM NiEDDA (Π [NiEDDA]) was determined by power saturation using a Bruker ER4123D dielectric resonator. The contrast parameter Φ is defined as $\Phi = \ln[\Pi (O_2)/\Pi (\text{NiEDDA})]$. Through calibration with 1-palmitoyl-2-stearoyl-(n-DOXYL)-sn-glycero-3-phosphocholine (Avanti Polar Lipids), Φ can be converted into immersion depth (Altenbach et al., 1994). Using this approach, we previously obtained the following relationship between immersion depth (d) and Φ for tubulated Folch membranes: d[Å] = 6.3*Φ − 3.9 (Gallop et al., 2006). We verified that this calibration was also applicable to the tubulated Folch membranes generated by the F-BAR protein.

Long-range distances were obtained from four-pulse DEER (Pannier et al., 2000) experiments that were performed on a Bruker Elexsys E 580 X-band pulsed EPR instrument fitted with a 3 mm split-ring (MS-3) resonator. The DEER experiment measures how the refocused echo of a given spin population is affected by dipolar interactions with other spins. This dipolar interaction gives rise to periodic oscillations in the spin echo intensity and their frequencies are a direct measure of interspin distance. Samples (~20 μl) were flash-frozen in the presence of either 30% glycerol or 30% sucrose and data were acquired at 78K. Identical distances were obtained in the presence of the different cryoprotectants. The observer pulse lengths for the $\Pi/2$ and Π pulses were 16 and 32 ns, respectively. The observe frequency was set to the maximum of the low-field absorption peak, while the ELDOR pump frequency was set to the maximum of the central absorption peak. Measurements were repeated with a repetition rate of 500 Hz. The total acquisition time ranged from 5 to 12 hr. Distance information from the dipolar time evolution data was generated using the DEERAnalysis 2006 package (freely available at http://www.mpip-mainz.mpg.de/~jeschke/distance.html) (Jeschke, 2002). Similar results were also obtained using DEFit, which was kindly provided by Dr. Peter G. Fajer (Florida State University). The background contribution from nonspecific protein-protein contacts was subtracted using a three-dimensional model for soluble F-BAR and a two-dimensional (planar) model for membrane-bound F-BAR (Hilger et al., 2005). Distances were fitted to a Gaussian distance distribution.

Negative-Stain Electron Microscopy

Sample protein was coincubated for 10 min with Folch fraction 1 liposomes and placed on glow discharged carbon-coated copper grids (CANEMCO-MARIVAC) for ~60 s. The grids were subsequently washed in buffer, then in water, and then stained with 2% uranyl acetate for 60 s. Grids were then dried and observed with a Phillips transmission electron microscope.

Supplemental Data

Supplemental Data include six figures and Supplemental Experimental Procedures and can be found with this article online at http://www.structure.org/cgi/content/full/15/7/839/DC1/.

ACKNOWLEDGMENTS

We would like to thank members of our labs for their expert advice and help in this study. This work was supported by the Medical Research Council (UK), and by an MRC Graduate Scholarship and a Trinity College External Research Studentship to W.M.H. R.L. was funded by the NIH (GM63915). We thank ESRF staff for assistance in data collection.

Received: May 1, 2007
Revised: May 15, 2007
Accepted: May 16, 2007
Published online: May 31, 2007

REFERENCES

Abrahams, J.P. (1997). Bias reduction in phase refinement by modified interference functions: introducing the γ function. Acta Crystallogr. D Biol. Crystallogr. *53*, 371–376.

Altenbach, C., Greenhalgh, D.A., Khorana, H.G., and Hubbell, W.L. (1994). A collision gradient method to determine the immersion depth of nitroxides in lipid bilayers: application to spin-labeled mutants of bacteriorhodopsin. Proc. Natl. Acad. Sci. USA *91*, 1667–1671.

Aspenström, P. (1997). A Cdc42 target protein with homology to the non-kinase domain of FER has a potential role in regulating the actin cytoskeleton. Curr. Biol. *7*, 479–487.

Bricogne, G., Vonrhein, C., Flensburg, C., Schiltz, M., and Paciorek, W. (2003). Generation, representation and flow of phase information in structure determination: recent developments in and around SHARP 2.0. Acta Crystallogr. D Biol. Crystallogr. *59*, 2023–2030.

Carlton, J., Bujny, M., Peter, B.J., Oorschot, V.M., Rutherford, A., Mellor, H., Klumperman, J., McMahon, H.T., and Cullen, P.J. (2004). Sorting nexin-1 mediates tubular endosome-to-TGN transport through coincidence sensing of high-curvature membranes and 3-phosphoinositides. Curr. Biol. *14*, 1791–1800.

CCP4 (Collaborative Computational Project, Number 4) (1994). The CCP4 suite: programs for X-ray crystallography. Acta Crystallogr. D Biol. Crystallogr. *50*, 760–763.

Chao, C.C., Chang, P.Y., and Lu, H.H. (2005). Human Gas7 isoforms homologous to mouse transcripts differentially induce neurite outgrowth. J. Neurosci. Res. *81*, 153–162.

Chitu, V., and Stanley, E.R. (2007). Pombe Cdc15 homology (PCH) proteins: coordinators of membrane-cytoskeletal interactions. Trends Cell Biol. *17*, 145–156.

Coyle, I.P., Koh, Y.H., Lee, W.C., Slind, J., Fergestad, T., Littleton, J.T., and Ganetzky, B. (2004). Nervous wreck, an SH3 adaptor protein that interacts with Wsp, regulates synaptic growth in *Drosophila*. Neuron *41*, 521–534.

de la Fortelle, E., and Bricogne, G. (1997). Maximum-likelihood heavy-atom parameter refinement for multiple isomorphous replacement and

multiwavelength anomalous diffraction methods. Methods Enzymol. *276*, 472–494.

Delfino, F.J., Stevenson, H., and Smithgall, T.E. (2006). A growth-suppressive function for the c-fes protein-tyrosine kinase in colorectal cancer. J. Biol. Chem. *281*, 8829–8835.

Emsley, P., and Cowtan, K. (2004). Coot: model-building tools for molecular graphics. Acta Crystallogr. D Biol. Crystallogr. *60*, 2126–2132.

Evans, P.R. (2006). Scaling and assessment of data quality. Acta Crystallogr. D Biol. Crystallogr. *62*, 72–82.

Ferguson, P.J., Bing, X., Vasef, M.A., Ochoa, L.A., Mahgoub, A., Waldschmidt, T.J., Tygrett, L.T., Schlueter, A.J., and El-Shanti, H. (2006). A missense mutation in pstpip2 is associated with the murine autoinflammatory disorder chronic multifocal osteomyelitis. Bone *38*, 41–47.

Foletta, V.C., Brown, F.D., and Young, W.S., III. (2002). Cloning of rat ARHGAP4/C1, a RhoGAP family member expressed in the nervous system that colocalizes with the Golgi complex and microtubules. Brain Res. Mol. Brain Res. *107*, 65–79.

Ford, M.G., Mills, I.G., Peter, B.J., Vallis, Y., Praefcke, G.J., Evans, P.R., and McMahon, H.T. (2002). Curvature of clathrin-coated pits driven by epsin. Nature *419*, 361–366.

Gallop, J.L., Jao, C.C., Kent, H.M., Butler, P.J., Evans, P.R., Langen, R., and McMahon, H.T. (2006). Mechanism of endophilin N-BAR domain-mediated membrane curvature. EMBO J. *25*, 2898–2910.

Grosse, J., Chitu, V., Marquardt, A., Hanke, P., Schmittwolf, C., Zeitlmann, L., Schropp, P., Barth, B., Yu, P., Paffenholz, R., et al. (2006). Mutation of mouse Mayp/Pstpip2 causes a macrophage autoinflammatory disease. Blood *107*, 3350–3358.

Habermann, B. (2004). The BAR-domain family of proteins: a case of bending and binding? EMBO Rep. *5*, 250–255.

Hilger, D., Jung, H., Padan, E., Wegener, C., Vogel, K.P., Steinhoff, H.J., and Jeschke, G. (2005). Assessing oligomerization of membrane proteins by four-pulse DEER: pH-dependent dimerization of NhaA Na^+/H^+ antiporter of *E. coli*. Biophys. J. *89*, 1328–1338.

Ho, H.Y., Rohatgi, R., Lebensohn, A.M., Le, M., Li, J., Gygi, S.P., and Kirschner, M.W. (2004). Toca-1 mediates Cdc42-dependent actin nucleation by activating the N-WASP-WIP complex. Cell *118*, 203–216.

Hubbell, W.L., Cafiso, D.S., and Altenbach, C. (2000). Identifying conformational changes with site-directed spin labeling. Nat. Struct. Biol. *7*, 735–739.

Itoh, T., and De Camilli, P. (2006). BAR, F-BAR (EFC) and ENTH/ANTH domains in the regulation of membrane-cytosol interfaces and membrane curvature. Biochim. Biophys. Acta *1761*, 897–912.

Itoh, T., Erdmann, K.S., Roux, A., Habermann, B., Werner, H., and De Camilli, P. (2005). Dynamin and the actin cytoskeleton cooperatively regulate plasma membrane invagination by BAR and F-BAR proteins. Dev. Cell *9*, 791–804.

Jeschke, G. (2002). Distance measurements in the nanometer range by pulse EPR. ChemPhysChem *3*, 927–932.

Jeschke, G., Koch, A., Jonas, U., and Godt, A. (2002). Direct conversion of EPR dipolar time evolution data to distance distributions. J. Magn. Reson. *155*, 72–82.

Jones, T.A., Zou, J.Y., Cowan, S.W., and Kjeldgaard, M. (1991). Improved methods for building protein models in electron density maps and the location of errors in these models. Acta Crystallogr. A *47*, 110–119.

Kakimoto, T., Katoh, H., and Negishi, M. (2006). Regulation of neuronal morphology by Toca-1, an F-BAR/EFC protein that induces plasma membrane invagination. J. Biol. Chem. *281*, 29042–29053.

Katoh, M., and Katoh, M. (2004). Identification and characterization of human FCHO2 and mouse Fcho2 genes in silico. Int. J. Mol. Med. *14*, 327–331.

Kim, L., and Wong, T.W. (1995). The cytoplasmic tyrosine kinase FER is associated with the catenin-like substrate pp120 and is activated by growth factors. Mol. Cell. Biol. *15*, 4553–4561.

Langen, R., Oh, K.J., Cascio, D., and Hubbell, W.L. (2000). Crystal structures of spin labeled T4 lysozyme mutants: implications for the interpretation of EPR spectra in terms of structure. Biochemistry *39*, 8396–8405.

Lee, S.H., Kerff, F., Chereau, D., Ferron, F., Klug, A., and Dominguez, R. (2007). Structural basis for the actin-binding function of missing-in-metastasis. Structure *15*, 145–155.

Leslie, A.G.W. (2006). The integration of macromolecular diffraction data. Acta Crystallogr. D Biol. Crystallogr. *62*, 48–57.

Lippincott, J., and Li, R. (2000). Involvement of PCH family proteins in cytokinesis and actin distribution. Microsc. Res. Tech. *49*, 168–172.

Masuda, M., Takeda, S., Sone, M., Ohki, T., Mori, H., Kamioka, Y., and Mochizuki, N. (2006). Endophilin BAR domain drives membrane curvature by two newly identified structure-based mechanisms. EMBO J. *25*, 2889–2897.

Mattila, P.K., Pykalainen, A., Saarikangas, J., Paavilainen, V.O., Vihinen, H., Jokitalo, E., and Lappalainen, P. (2007). Missing-in-metastasis and IRSp53 deform $PI(4,5)P_2$-rich membranes by an inverse BAR domain-like mechanism. J. Cell Biol. *176*, 953–964.

McMahon, H.T., and Gallop, J.L. (2005). Membrane curvature and mechanisms of dynamic cell membrane remodelling. Nature *438*, 590–596.

Millard, T.H., Bompard, G., Heung, M.Y., Dafforn, T.R., Scott, D.J., Machesky, L.M., and Futterer, K. (2005). Structural basis of filopodia formation induced by the IRSp53/MIM homology domain of human IRSp53. EMBO J. *24*, 240–250.

Murshudov, G.N., Vagin, A.A., and Dodson, E.J. (1997). Refinement of macromolecular structures by the maximum-likelihood method. Acta Crystallogr. D Biol. Crystallogr. *53*, 240–255.

Pannier, M., Veit, S., Godt, A., Jeschke, G., and Spiess, H.W. (2000). Dead-time free measurement of dipole-dipole interactions between electron spins. J. Magn. Reson. *142*, 331–340.

Pasder, O., Shpungin, S., Salem, Y., Makovsky, A., Vilchick, S., Michaeli, S., Malovani, H., and Nir, U. (2006). Downregulation of Fer induces PP1 activation and cell-cycle arrest in malignant cells. Oncogene *25*, 4194–4206.

Peter, B.J., Kent, H.M., Mills, I.G., Vallis, Y., Butler, P.J., Evans, P.R., and McMahon, H.T. (2004). BAR domains as sensors of membrane curvature: the amphiphysin BAR structure. Science *303*, 495–499.

Qualmann, B., Roos, J., DiGregorio, P.J., and Kelly, R.B. (1999). Syndapin I, a synaptic dynamin-binding protein that associates with the neural Wiskott-Aldrich syndrome protein. Mol. Biol. Cell *10*, 501–513.

Schilling, K., Opitz, N., Wiesenthal, A., Oess, S., Tikkanen, R., Muller-Esterl, W., and Icking, A. (2006). Translocation of endothelial nitric-oxide synthase involves a ternary complex with caveolin-1 and NOSTRIN. Mol. Biol. Cell *17*, 3870–3880.

Tarricone, C., Xiao, B., Justin, N., Walker, P.A., Rittinger, K., Gamblin, S.J., and Smerdon, S.J. (2001). The structural basis of Arfaptin-mediated cross-talk between Rac and Arf signalling pathways. Nature *411*, 215–219.

Tsujita, K., Suetsugu, S., Sasaki, N., Furutani, M., Oikawa, T., and Takenawa, T. (2006). Coordination between the actin cytoskeleton and membrane deformation by a novel membrane tubulation domain of PCH proteins is involved in endocytosis. J. Cell Biol. *172*, 269–279.

Uson, I., and Sheldrick, G.M. (1999). Advances in direct methods for protein crystallography. Curr. Opin. Struct. Biol. *9*, 643–648.

Weissenhorn, W. (2005). Crystal structure of the endophilin-A1 BAR domain. J. Mol. Biol. *351*, 653–661.

Accession Numbers

The structure of hFCHo2 F-BAR domain has been deposited in the Protein Data Bank under ID code 2V0o.

